AC susceptibility of the dilute PdFe system

1992 J. Phys.: Condens. Matter 4 10385

(http://iopscience.iop.org/0953-8984/4/50/027)

J. Phys.: Condens. Matter 4 (1992) 10385–10398. Printed in the UK

AC susceptibility of the dilute PdFe system

Z Wang, H P Kunkel and Gwyn Williams
Department of Physics, University of Manitoba, Winnipeg, R3T 2N2, Canada

Received 9 June 1992, in final form 5 October 1992

Abstract. We present a detailed study of the field- and temperature-dependent AC susceptibility of Pd containing between 0.35 and 2.4 at.% Fe which reveals a number of unusual features of this previously well studied system. While all of the samples examined become ferromagnetic at low temperature, there are marked differences in the critical behaviour at different compositions. Near 1.4 at.% Fe this system displays near-Heisenberg-model exponents ($\gamma = 1.39$, $\beta = 0.365$, $\delta = 4.8$) with little exchange-bond disorder. By contrast, at both higher and lower composition, effective exponent values that vary with both temperature and field are found, a result which is consistent with significant exchange-bond disorder. At lower composition, fluctuations in the exchange-coupling strength can arise due to oscillations that occur in the conduction-electron polarization at large distances, but at higher composition an alternative mechanism for exchange competition must exist. We suggest that direct Fe–Fe near-neighbour exchange is the source of this competition, and discuss other properties of the PdFe system that support this suggestion.

1. Introduction

PdFe is probably the most intensively studied giant-moment system, having been investigated by a wide range of transport, magnetic, specific-heat, Mössbauer and resonance methods [1–11]. Its composition–critical temperature diagram—summarized in figure 1—is consequently well established, covering some five decades in composition from 2 ppm to 25 at.% Fe (Pd_3Fe; both spatially ordered and disordered). At low Fe concentration ($c \leqslant 100$ ppm) the system is a spin glass, with a critical temperature T_{sg} scaling approximately linearly with composition at a rate $T_{sg}/c \approx 75$ μK/ppm Fe [2,3]. The ferromagnetic percolation threshold between exchange-enhanced giant Fe moments occurs in the vicinity of 0.01 to 0.1 at.% Fe, although even above this composition a significant number of these moments are not coupled by direct overlap to the percolation 'backbone', they still reside in regions where the net conduction-electron spin polarization is oscillatory. Such a picture is confirmed by the presence of a strong negative component in the magnetoresistance at temperatures well below the Curie temperature T_C in this composition range [12]. Despite such complications, the ordering temperature increases as c^2 throughout the region between 0.01 and $\sim$ 0.4 at.% Fe. Somewhat surprisingly, in view of both the concentration range and the temperature interval into which T_C falls, data acquired beyond 0.4 at.% Fe appear to exhibit perhaps the greatest scatter; nevertheless the phase diagram indicates a linear increase in T_C with composition (for $c \geqslant 0.4$ at.%), but at two different rates; between approximately 0.4 and 2 at.% Fe the line drawn corresponds to $T_C/c = 39$ K/at.%, while at higher concentration ($3 \leqslant c < 25$ at.%) $T_C/c \approx 23$ K/at.%. A possible origin for this

0953-8984/92/5010385+14$07.50

shift will be discussed later in terms of a change in the dominant coupling mechanism. At this point it is worthwhile recalling that this shift has been noted previously [13], and its presence correlates with changes in other properties of this system in the vicinity of 2 at.% Fe. Specifically, the concentration dependence of the acoustic spin-wave stiffness D [14] changes abruptly near this composition, and the mean impurity moment—although scattered in value principally between 9 and $12\mu_B$ per impurity below 1 at.% Fe—falls to significantly lower values at higher concentration (inset in figure 1). Furthermore, not only does the net magnetic component in the resistivity $\Delta\rho_m(=\rho_m(T)-\rho_m(0);\ \rho_m(T)=\rho_{Alloy}(T)-\rho_{Pd}(T))$ vary anomalously near this composition [13], but its limiting low-temperature variation changes from $\rho_m(T \ll T_C) \propto T^{3/2}$ to $\propto T^2$ [13, 15] (these temperature dependences being characteristic of conduction-electron–acoustic-magnon scattering without [15, 16] and with [17, 18] wavevector conservation, respectively). Many of these effects also appear to correlate with the onset of a nearly homogeneous Pd d band polarization beyond 2–3 at.% Fe [13, 19].

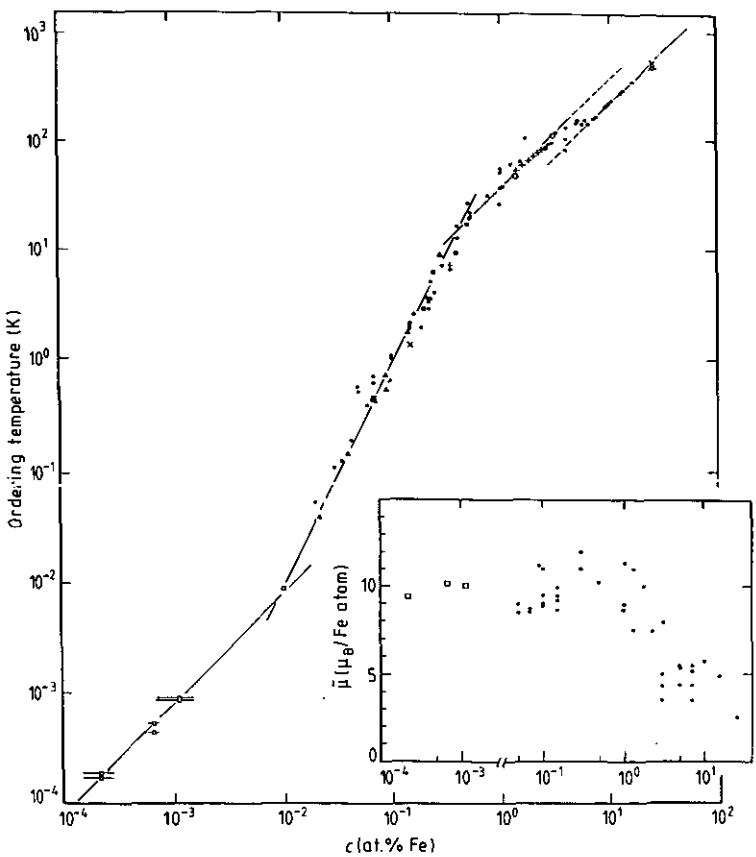

Figure 1. A summary of various estimates for the ordering temperature (in K) of PdFe alloys plotted against composition c (in atomic %) on a double logarithmic scale. Data are from: (□) [2], (●) [1], (○) [4], (×) [6], (⊠) [8], (▼) [9], (■) [10], (◆) [5], (▲) [7], (+) present data. Inset: the average moment per Fe atom (in μ_B) as a function of composition.

Below we present a detailed study of the temperature and biasing-field dependent AC susceptibility of several samples, with composition between 0.35 and 2.4 at.% Fe (i.e. near the onset of a homogeneous d band polarization), in the vicinity of their critical temperatures. Attempts are made to relate differences in both the measured critical behaviour and various other properties indicated above, with modification introduced into the exchange-bond distribution by varying the composition.

2. Experimental details

Seven PdFe samples containing between 0.35 and 2.4 at.% Fe were prepared by arc melting using 99.999% pure Pd wire and 99.99% pure Fe rod (both supplied by Johnson Matthey, London). Initially a master alloy containing 2.4 at.% Fe was prepared and homogenized by inverting and remelting several times; melting losses were negligibly small. Following cold rolling (between protective Melinex sheets) this specimen was briefly etched to remove any surface contamination; subsequently samples containing 2.2, 2.0, 1.8, 1.6, 1.4 and 0.35 at.% Fe were made by successive dilution from the master alloy following the above procedure. Susceptibility specimens of approximate dimensions $1.7 \times 0.2 \times 0.01$ cm^3 (with rounded corners) were cut from cold-rolled sheets; following surface etching they were annealed for 24 h at 1000 °C in 10^{-6} Torr and quenched in ice-water immediately prior to measuring. The in-phase component of the susceptibility of these samples was recorded continuously using a previously described phase-locked susceptometer [20], with an AC driving field of 5 μT RMS at 2.4 kHz applied along the largest specimen dimension. A collinearly mounted solenoid was used to null the vertical component in the earth's field (~ 53 μT) during cooling and to apply static biasing fields ($\mu_0 H_a$) between 0 and 0.1 T. The specimen temperature was measured with a Au +0.03 at.% Fe versus Chromel P thermocouple.

The true susceptibility $\chi_t(H_i, T)$ was calculated in the usual way [21]

$$\chi_t(H_i, T) = \partial M/\partial B_i = \chi_m(H_a, T)/(1 - N\chi_m(H_a, T)) \qquad (1)$$

from the measured response $\chi_m = \partial M/\partial B_a$, with the internal field $B_i = \mu_0 H_i$ being found from the applied magnetic excitation H_a using $H_i = H_a - NM$. The demagnetizing factor N was estimated by approximating each sample by an ellipsoid with principal axes equal to the corresponding dimension and evaluating the appropriate elliptic integral [22]. Such a procedure sets an upper limit on N [23, 24] which, for the samples studied here, lies in the range 7×10^{-6}–8×10^{-5} (when $\chi_m(H_a, T)$ is the susceptibility per unit mass), leading to a demagnetizing factor correction through equation (1) in the range 10–20%.

3. Results and discussion

3.1. General features

In all samples studied, the zero-field AC susceptibility $\chi_t(0, T)$ increases rapidly with decreasing temperature as the Curie temperature T_C is approached from above. $\chi_t(0, T)$ reaches a maximum just below T_C—the Hopkinson or principal maximum—at a temperature designated T_H; on further cooling below T_H, $\chi_t(0, T)$ decreases slowly. The correction for demagnetizing effects, equation (1), is consequently a maximum at T_H, lying in the range 10–20%, so that the true susceptibility does not diverge at

T_C for the sample geometry and driving fields utilized here (the former having been specifically chosen to minimize such corrections). The application of static biasing fields of increasing magnitude progressively reduces both the temperature T_H and the susceptibility $\chi_t(H, T_H)$ at the Hopkinson maximum, and this facilitates the observation of secondary/critical peaks as discussed below. The behaviour of these critical peaks is qualitatively similar in all samples studied—they increase in temperature *above* T_C and decrease in amplitude as the static biasing field increases. However, quantitative analysis of this behaviour reveals marked differences as the Fe composition is changed. These differences are discussed below.

3.2. Pd + 1.4 at.% Fe; a nearly ideal system

Figure 2, in which the true susceptibility $\chi_t(H_i, T)$ is plotted against temperature for various (estimated) internal fields, shows the behaviour of the secondary/critical peak structure discussed above. As reported previously for a number of other systems [22], and in agreement with the predictions of the static scaling law [22,25], the temperature T_m of the critical peaks increases with increasing field according to

$$t_m = (T_m - T_C)/T_C \propto (H_i/T_C)^{1/(\gamma+\beta)} \tag{2}$$

while the magnitude of the susceptibility at these (secondary) maxima decreases with increasing field h ($\propto H_i/T_C$) as:

$$\chi_t(h, t_m) \propto h^{1/\delta-1}. \tag{3}$$

Equations (2) and (3), along with the usual dependence of the zero-field susceptibility on (reduced) temperature above T_C,

$$\chi_t(0, t) \propto t^{-\gamma} \qquad t = (T - T_C)/T_C \tag{4}$$

form the basis for the analysis of the critical behaviour carried out below.

An initial estimate for the Curie temperature T_C is made by plotting the peak temperature T_m (evident in figure 2) against $\sqrt{H_i}$ (for Heisenberg-model HM exponents [26], $(\gamma+\beta)^{-1} \approx 0.5$). Using this initial estimate, double logarithmic plots of t_m against H_i (a test of equation (2)) and $\chi_t(0, t)$ against t (a test of equation (4)) are made, and then small adjustments, ΔT_C, in T_C ($\Delta T_C/T_C \leqslant 2$–$3 \times 10^{-3}$) are introduced until a consistent set of plots, similar to those shown in figures 3 and 4, are obtained. Not only do the straight-line portions of such plots confirm the power-law dependences predicted by equations (2) and (4) (over the appropriate reduced temperature regime) but their slopes enable exponent values to be estimated. Figure 4 yields $\gamma = 1.36 \pm 0.03$ ($10^{-2} \leqslant t \leqslant 2 \times 10^{-1}$) and from figure 3 the cross-over exponent† is estimated at $(\gamma + \beta)^{-1} = 0.57 \pm 0.01$ from which $\beta = 0.39(5) \pm 0.01(5)$. Figure 5, in which the peak susceptibility $\chi_t(h, t_m)$ is plotted against the internal field‡ H_i, tests the remaining power-law of equation (3). Close inspection of this figure reveals slight curvature (the slope decreases

† The maxima evident in figure 2 mark the boundary, in the (h, t) plane, below which the response is field-dominated, and above which it is temperature-dominated [27]. This boundary is referred to consequently as the cross-over line (shown schematically by the dashed curve), and the associated exponent $(\gamma+\beta)^{-1}$ is termed the cross-over exponent.

‡ The internal field is obtained from the applied field using the calculated demagnetization factor, in conjunction with the magnetization found from numerical integration of the measured susceptibility, as discussed previously [21].

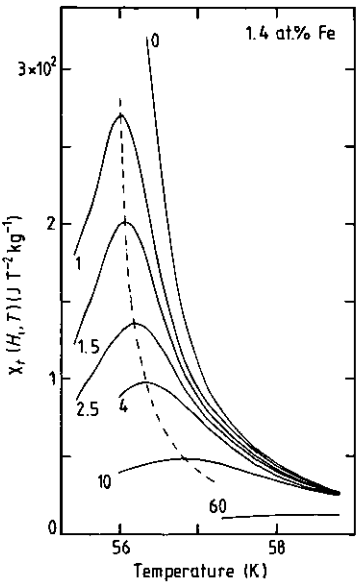

Figure 2. The true susceptibility $\chi_t(H_i, T)$ (in J T^{-2} kg^{-1}) (corrected for background and demagnetizing effects) plotted against temperature (in K) for Pd+1.4 at.% Fe. The number marked against each curve is the estimated static biasing field $\mu_0 H_i$ (in mT); The broken curve represents the cross-over line.

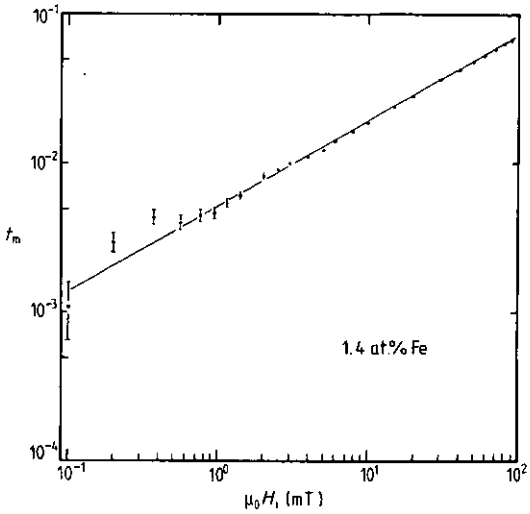

Figure 3. The reduced temperature t_m of the cross-over line plotted against the internal field $\mu_0 H_i$ (in mT) on a double logarithmic scale for the 1.4 at.% Fe sample. The line drawn has a slope of $(\gamma + \beta)^{-1} = 0.57$. The error bars correspond to ±25 mK.

marginally in magnitude as the field increases), indicating that this power-law prediction with a unique exponent δ is not strictly obeyed in this sample. Similar, though more marked, behaviour in which the effective exponent $\delta^*(H)$ decreases with increasing field has been reported previously in a number of systems [22], and can be attributed to the presence of an exchange-bond distribution of finite width [28,29]. Here the slope of the low-field data yield an exponent value of $\delta = 4.5 \pm 0.15$ ($10^{-4} \leqslant \mu_0 H_i < 3 \times 10^{-3}$ T) with the effective exponent $\delta^*(H)$ falling to slightly lower value of 4.0 ± 0.1 near 0.1 T. The low-field value of δ, when combined with the estimate of γ from figure 4 and the Widom equality [30]

$$\gamma = \beta(\delta - 1) \tag{5}$$

yields a value for β of $\beta = 0.39 \pm 0.02$ in good agreement with that found from the cross-over exponent. These exponent values are quite close to those predicted by the isotropic, 3-dimensional HM ($\gamma = 1.386$, $\beta = 0.365$, $\delta = 4.80$) [26].

The relatively small decline in the effective exponent $\delta^*(H)$ with increasing field is consistent with an exchange-bond distribution for which the ratio of width (ΔJ) to mean value J_0 satisfies $\Delta J/J_0 \ll 1$. This conclusion is also consistent with the behaviour of the effective Kouvel–Fisher susceptibility exponent [31]

$$\gamma^*(T) = \mathrm{d}\ \ln(\chi_t(0,t))/\mathrm{d}\ \ln(t) \tag{6}$$

shown in the insert in figure 4. In systems with marked exchange-bond disorder this latter effective exponent exhibits a non-monotonic variation with temperature,

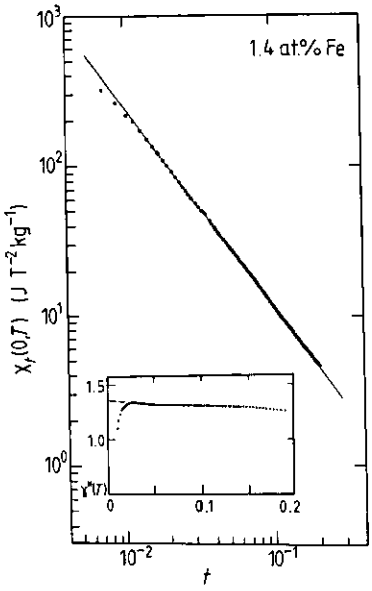

Figure 4. The true zero-field susceptibility $\chi_t(0,T)$ in (J T^{-2} kg^{-1}) plotted against reduced temperature t on a double logarithmic scale for the 1.4 at.% Fe specimen; the line drawn corresponds to $\gamma = 1.36$. The insert shows the effective susceptibility exponent $\gamma^*(T)$ plotted against t on a linear scale.

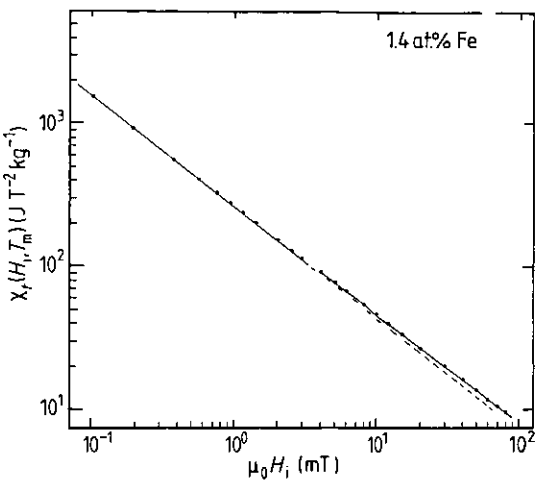

Figure 5. The critical peak susceptibility $\chi_t(H_i, T_m)$ (in J T^{-2} kg^{-1}) (i.e. the susceptibility along the cross-over line) plotted against the internal field $\mu_0 H_i$ (in mT) on a double logarithmic scale for the 1.4 at.% Fe sample. The lines drawn yield the δ-values shown in table 1.

displaying a characteristic maximum above T_C [32,33]. This contrasts with the behaviour evident here and in 'pure' systems in which $\gamma^*(T)$ falls monotonically from near HM values close to T_C towards a mean-field value of $\gamma^*(T) \approx 1$ at high temperature.

Both the rapid fall in $\gamma^*(T)$ below $t \approx 10^{-2}$ and the departure of $\chi_t(0,t)$ from a power-law dependence near the same reduced temperature, evident in figure 4 for this PdFe sample, have been reported previously and discussed for a number of other systems [21,34]. They are a direct consequence of the behaviour discussed in section 3.1., i.e. the failure of the measured response to approach the demagnetization-limited value close to T_C. This result is a manifestation of anisotropy effects usually associated with spin–orbit coupling (which, however weak, will *eventually* prevent the true susceptibility from increasing without limit sufficiently close to T_C). These effects become evident here due to the use of samples with very small demagnetizing factors. (As discussed previously [22,38], if the measured susceptibility reaches the demagnetization-limited value, it is inferred that the true susceptibility diverges; correspondingly the internal field ($H_i = H_a - NM$) is zero. In an experiment measuring the AC susceptibility, since the driving field oscillates, so will the induced magnetization if the above condition is to be met. Smaller N-values thus demand larger oscillations in M to maintain $H_i = 0$. Consequently a greater magnetization reversal is required in small-N specimens if the above condition is to be satisfied. This reversal is opposed by anisotropy effects which are therefore more likely to be observed in samples with small demagnetization factors.) An extrapolation of the variation of $\gamma^*(t)$ with temperature from the region $t \geqslant 10^{-2}$ suggests, however,

from the power-law behaviour evident, for $10^{-2} \leqslant t \leqslant 2 \times 10^{-1}$, in the main body of figure 4.

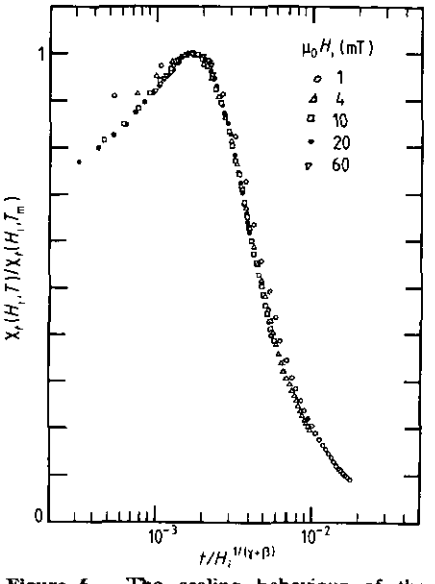

Figure 6. The scaling behaviour of the field and temperature dependent susceptibility of the 1.4 at.% sample (—the susceptibility normalized to its peak value, plotted against the (inverse) argument of the scaling function).

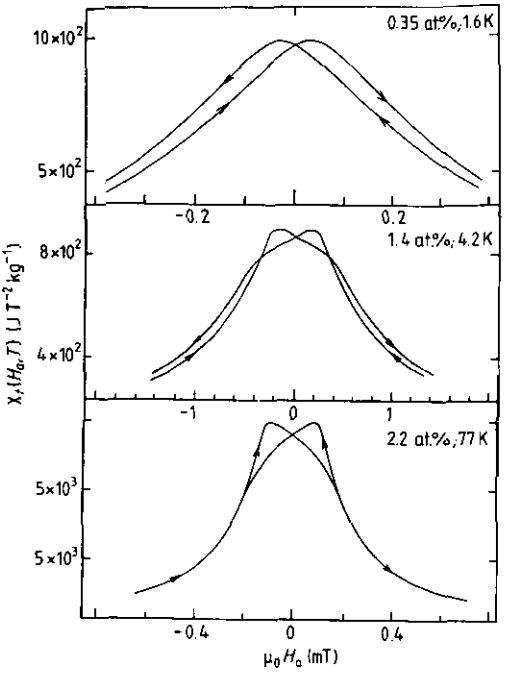

Figure 7. Butterfly loops—$\chi_t(H_a, T)$ (in J T^{-2} kg^{-1}) plotted against applied field $\mu_0 H_a$ (in mT) at various fixed temperatures—for three selected samples.

A final, conclusive demonstration of scaling behaviour in this sample is provided by figure 6. Here it is shown that the entire field- and temperature-dependent response $\chi(h,t)$ can be collapsed onto a single curve. This is achieved by plotting $\chi(h,t)/\chi(h,t_m)$ (the susceptibility measured in any fixed field h, normalized to its peak value) against the (inverse) of the usual argument of the scaling function, $t/h^{1/(\gamma+\beta)}$ [22].

Next we return to the question of anisotropy in this system. The expectation that spin–orbit mediated magnetocrystalline anisotropy should be small in PdFe is based on the results of measurements of the spontaneous resistive anisotropy (SRA) [35]. The SRA, essentially the difference in resistance (extrapolated to zero induction) of a single-domain ferromagnetic conductor when the magnetization lies parallel or perpendicular to the current direction, vanishes when there is no spin–orbit coupling present [36, 37]. The observation of a vanishing SRA in the limit of low Fe concentration has been interpreted as indicating the absence of an orbital moment on Fe impurities in Pd (in contrast to the case of Ni or Co impurities). As a corollary, the appearance of a finite SRA as the Fe concentration is increased presumably reflects the presence of spin–orbit coupling in the impurity-induced exchange-split Pd d bands. Furthermore, in giant-moment systems where the d band polarization makes a significant contribution to the total moment/magnetization, it might therefore be expected that the host spin–orbit

coupling would be instrumental in producing an anisotropy (albeit indirect for impurities lacking an orbital moment, and thus possibly weakened).

This suggestion of a rather weak anisotropy in PdFe is also supported by the data shown in figures 3 and 5. Specifically the ability of internal fields as low as 10^{-4} T to resolve critical peak structure indicates that the critical component in the response dominates the regular/technical component in very low field. In 'hard' magnetic material the regular/technical response (usually attributed to coherent rotation and/or domain-wall motion) is not driven to (technical) saturation in low fields, so that much higher fields are required before the critical response dominates [34]. The converse appears to be true here. The data presented in figure 7 indicate directly the 'soft' magnetic character of this system; here 'butterfly loops' ($\chi(H, T)$ versus H_a at various fixed temperatures) enable the coercive field to be estimated from the splitting between the susceptibility maxima. These fields are listed in table 2 for various fixed temperatures; they are clearly small (though non-zero) for Pd+1.4 at.% Fe. One further comment on these butterfly loops is necessitated by their slightly unusual character; only those acquired for the 0.35 at.% Fe sample are conventional in the sense that the susceptibility maxima occur in reverse fields [23]. Those measured on samples with 1.4 at.% Fe or more exhibit susceptibility maxima in *forward* fields, resembling Perminvars and 68 Permalloy [23], where such effects are attributed to the presence of a domain structure with a sensitivity to heat treatment and strain, resulting from a small anisotropy constant. This behaviour is not expected to influence the critical response (and the differences between the 1.4 at.% Fe and more concentrated samples appear to confirm this), specifically because the coercive field is expected to vanish near T_C (as can be seen from the data in table 2); nevertheless, it does mean that the H_c estimates are somewhat indirect in all cases except the 0.35 at.% Fe sample.

To summarize the behaviour of the 1.4 at.% sample, it exhibits well defined critical behaviour with near HM exponents (shown in table 1), a narrow exchange-bond distribution and weak anisotropy effects. There is only one previous measurement of exponent values for samples in the composition range investigated here; Kouvel and Comly [4] report $\gamma = 1.40$, $\beta = 0.46$, $\delta = 4.06$ for a sample of the same nominal composition (1.4 at.% Fe), although probably of lower actual composition (T_C was reported as 50.25 K, compared with 55.75 K in the present sample). In view of the effects of composition on the effective/apparent exponent values (discussed below), these small differences in the γ and β values appear reasonable; the rather lower value reported for δ is likely attributable (judging from the behaviour shown in figure 5) to the use of fields ($\mu_0 H_a$) in excess of 50 mT [4].

3.3. Effects of compositional variations

3.3.1. Pd + 0.35 at.% Fe. A detailed analysis of the critical peak behaviour in this sample is summarized in figures 8 to 10. Figure 8 reproduces the field and temperature dependence of the cross-over line (t_m versus h); the solid line drawn in this figure (which can be extended to fit all data points, including those below $t_m \simeq 5 \times 10^{-2}$) demonstrates that within experimental uncertainty it is possible to fit these data to a single power law (equation (2)) with unique exponent values over the entire field range examined ($4 \times 10^{-5} \leqslant \mu_0 H_i \leqslant 0.1$ T). This line, however, corresponds to non-HM exponent values as its slope yields $(\gamma + \beta)^{-1} = 0.54(3) \pm 0.01$ from which $\gamma + \beta = 1.84(2) \pm 0.03(4)$. We have chosen not to extend this solid line to low field and temperature values, but (for reasons discussed below) to indicate, via the dashed line in this figure, that data below $t_m \simeq 5 \times 10^{-2}$ do not preclude (within experimental uncertainty) *asymptotic*

Table 1. Summary of effective exponent values and the temperature/field intervals over which these are appropriate, for the PdFe alloys studied. Susceptibility exponent: t^a, the reduced temperature at which $\gamma^*(t)$ reaches the HM value, of 1.39 (except for the 1.4 at.% sample—see text); γ^*_{max}, the maximum value of $\gamma^*(t)$ achieved at reduced temperature t_{max}. Cross-over line: LOW TEMP (†) denotes consistency with HM values (0.57), achieved below t^b_m; OVERALL refers to the principal behaviour of the cross-over line. $\delta^*(H)$: LOW FIELD denotes the value of the effective exponent and the internal field *below* which this value is reached; HIGH FIELD denotes the value of the effective exponent and internal field *above* which this effective exponent is valid.

SAMPLE (at.% Fe)	T_c (K)	SUSCEPTIBILITY EXPONENT				CROSS-OVER LINE			$\delta^*(H)$			
						LOW TEMP		OVERALL	LOW FIELD		HIGH FIELD	
		$\gamma^*(t)$	t^a	γ^*_{max}	t_{max}	t^b_m	$(\gamma+\beta)^{-1}$	$(\gamma+\beta)^{-1}$	H(mT)	$\delta^*(H)$	$\delta^*(H)$	H(mT)
0.35	7.50±0.03	1.39	2×10^{-2}	1.8±0.1	6×10^{-2}	$<3\times10^{-2}$	0.57†	0.54(3)±0.01	<1.5	3.4±0.1	3.1±0.1	>3
1.4	55.6±0.1	1.37±0.01	0	1.36±0.03	$<2\times10^{-1}$	10^{-3}	0.57±0.01	0.57±0.01	<2.5	4.5±0.1	4.0±0.1	>4
1.6	61.5±0.2	1.39	2×10^{-2}	3.3±0.1	6×10^{-2}	$<1.5\times10^{-2}$	0.57†	0.50±0.01	<1.5	4.45±0.1	2.9±0.1	>2.5
1.8	69.1±0.2	1.39	4×10^{-2}	3.2±0.1	10×10^{-2}	–	–	0.50±0.02	<4	4.0±0.1	2.6±0.1	>5
2.0	75.4±0.3	1.39	3×10^{-2}	3.3±0.1	7×10^{-2}	$<10^{-2}$	0.57†	0.50±0.02	<2.5	3.2±0.1	2.4±0.1	>4
2.2	80.6±0.5	1.39	1.5×10^{-2}	3.2±0.1	5×10^{-2}	$<1.5\times10^{-2}$	0.57†	0.51±0.02	<4	3.0±0.1	2.5±0.1	>5
2.4	86.6±0.5	1.39	1.5×10^{-2}	3.6±0.1	4×10^{-2}	$<1.7\times10^{-2}$	0.57†	0.53±0.03	<3	3.0±0.1	2.7±0.1	>4

Table 2. Estimate of the coercive field $\mu_0 H_c$ (from butterfly loops, similar to those shown in figure 7) and the lowest field $\mu_0 H_0$ necessary to first resolve critical peak structure.

Sample (at.% Fe)	$\mu_0 H_0$ (mT)	$\mu_0 H_c$ (mT)			
		77 K	58 K	4.2 K	1.6 K
0.35	4.4×10^{-2}	—	—	1.7×10^{-2}	3.2×10^{-2}
1.4	10^{-1}	—	—	1.6×10^{-1}	
1.6	1	—	—	1.8×10^{-1}	
1.8	2.5	—	—	2.7×10^{-1}	
2.0	1.5	$\leqslant5\times10^{-3}$	2.4×10^{-1}	2.7×10^{-1}	
2.2	2	9×10^{-2}	2.4×10^{-1}	2.4×10^{-1}	
2.4	1	1.5×10^{-1}	1.7×10^{-1}	2×10^{-1}	

exponent values consistent with model predictions [22]. If this interpretation is accepted, then the resulting curvature in this plot would indicate effective exponent values ($\gamma^*(t)$ and $\beta^*(t)$) which *increase* with increasing temperature immediately above T_C. Such behaviour has been reported previously in a number of disordered systems [32,33], and direct confirmation of this for the susceptibility exponent $\gamma^*(t)$ in the present system is provided in figure 9. The curvature evident in figures 8 and 9 is qualitatively consistent with that suggested by models incorporating exchange-bond disorder [28,29].

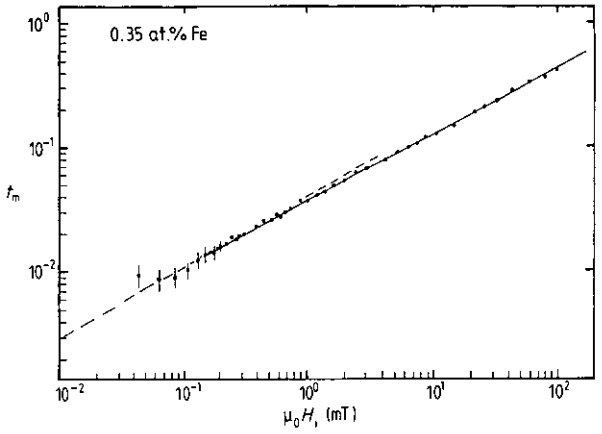

Figure 8. The reduced temperature t_m of the cross-over line plotted against the internal field $\mu_0 H_i$ (in mT) on a double logarithmic scale for the 0.35 at.% Fe sample. The solid line represents the overall behaviour of this line while the dashed line corresponds to HM-value exponents.

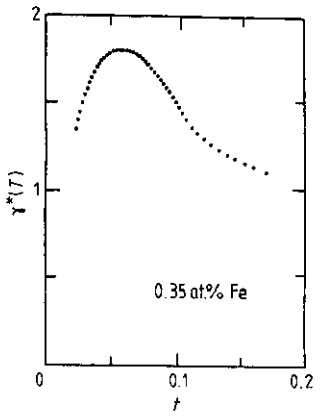

Figure 9. The Kouvel–Fisher effective susceptibility exponent $\gamma^*(T)$ plotted against reduced temperature t for the 0.35 at.% Fe specimen.

These results present obvious difficulties in extracting a reliable value for β from the slope of the cross-over line, as the data in figure 8 are not sufficiently precise to enable a point value for $\gamma^*(t) + \beta^*(t)$ to be estimated and compared with the data in figure 9. Using an 'average' $\langle\gamma^*(t)\rangle \simeq 1.45$ over the above temperature range would yield $\beta \simeq 0.39$, in agreement with the 1.4 at.% sample, but such a choice of an average γ is not easily justified. Combining a 3D HM value of $\gamma = 1.386$, valid experimentally only in the vicinity of $t \simeq 2 \times 10^{-2}$, with the overall characteristics of the cross-over line, yields $\beta = 0.46$; the latter is well above its corresponding model prediction and the value found in the 1.4 at.% sample. We reiterate therefore that the data in figures 8 and 9 do not preclude asymptotic values for both γ and β that agree with model predictions [26], provided the behaviour of $\gamma^*(t)$ near $t = 2 \times 10^{-2}$ is taken as indicating its asymptotic value (notwithstanding the fall in $\gamma^*(t)$ at lower reduced temperature, discussed above for the 1.4 at.% sample). Thus while there is some doubt about precise asymptotic exponent values, the influence of bond disorder in invalidating the power-law predictions of equations (2) and (4) (with unique exponents) is clear.

Further evidence for the presence of bond disorder can be found in figure 10, which yields an effective exponent $\delta^*(H) = 3.1 \pm 0.1$ above $\mu_0 H_i \simeq 5 \times 10^{-3}$ T, increasing with decreasing field to $\delta^*(H) = 3.4 \pm 0.1$ near $\mu_0 H_i = 10^{-4}$ T. This trend is again consistent with that suggested by models incorporating exchange bond disorder [28,29]. Even with marked bond disorder, however, one might nevertheless expect $\delta^*(H)$ to increase to near-HM values ($\delta = 4.80$) at low fields (cf PdMn [22,39]). However, it must

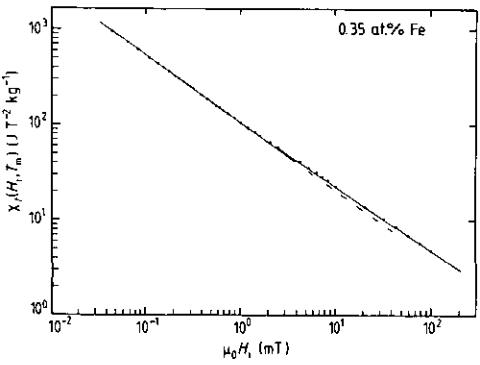

Figure 10. The critical peak susceptibility $\chi_t(H_i, T_m)$ (in J T^{-2} kg^{-1}) plotted on a double logarithmic scale against the internal field $\mu_0 H_i$ (in mT) for the 0.35 at.% Fe alloy. The lines drawn yield the δ-values shown in table 1.

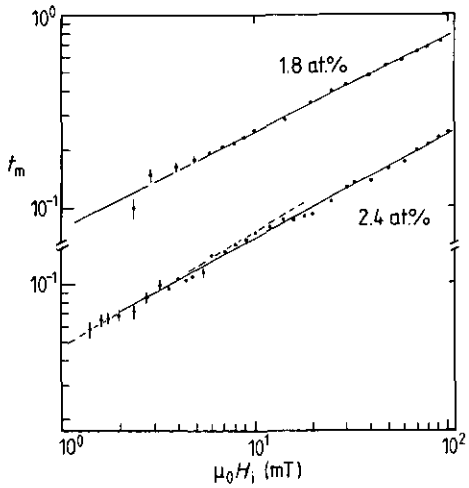

Figure 11. The reduced temperature t_m plotted against internal field $\mu_0 H_i$ (in mT) for the 1.8 and 2.4 at.% samples. The lines drawn yield the $(\gamma + \beta)^{-1}$ values reproduced in table 1.

be remembered that, in spite of the use of a sample geometry which results in low values for the demagnetization factor N, estimates for the internal field—when this field falls below 10^{-4} T—become increasingly uncertain due to the lack of an exactly calculable value for N. Support for the suggestion that such uncertainties might mask further increases in $\delta^*(H)$ as H_i falls comes from the use of the Widom relationship, which indicates δ values in the range 4.0 to 4.8; here the lowest δ-estimate, obtained using the largest β-value (0.46), is still considerably above that obtained from the low-field region of figure 10.

3.3.2. Samples containing between 1.6 and 2.4 at.% Fe. While the zero-field response of all the specimens studied is basically similar, significant differences in the field- and temperature-dependent behaviour of the critical peaks are observed, typified by the data summarized in figures 11 to 13 for the 1.8 and 2.4 at.% samples. Two principal conclusions can be drawn from these latter figures. First, considerably larger fields are required to initially resolve critical peak structure in specimens containing 1.6 at.% Fe or more (these fields, $\mu_0 H_0$, are listed in table 2, and can be compared with the various coercive-field estimates also summarized there; a large H_0 indicates a 'technically' hard sample since non-critical (i.e. technical) components in the response are not driven to saturation in low field, thus allowing the critical component to dominate). Second, various double-logarithmic plots display marked curvature, indicative of effective exponents with strong field- and temperature-dependence frequently attributed to extensive exchange-bond disorder.

For the data sets shown, at 1.8 at.% Fe the internal field needed to first resolve critical-peak structure is near 2.5 mT (some twenty-five times larger than at 1.4 at.%); $\delta^*(H) \simeq 2.6$ for $\mu_0 H_i > 5$ mT, increasing sharply with decreasing field to $\delta^*(H) = 4.0$ below $\mu_0 H_i = 4$ mT. Whether $\delta^*(H)$ continues to increase toward a HM value with further decreases in field is uncertain, as the marked increase in H_0 noted above prohibits such observations. Similar comments apply to the cross-over line; $(\gamma^* +$

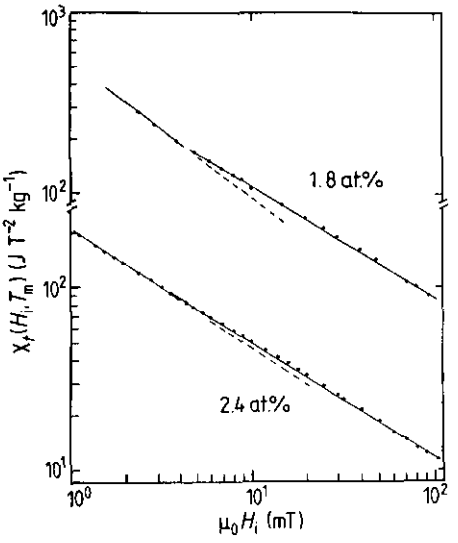

Figure 12. Double logarithmic plots of the critical peak susceptibility $\chi_t(H_i, T_m)$ (in J T^{-2} kg^{-1}) versus internal field $\mu_0 H_i$ (in mT) for the 1.8 and 2.4 at.% specimens. The δ-values found from the lines drawn are summarized in table 1.

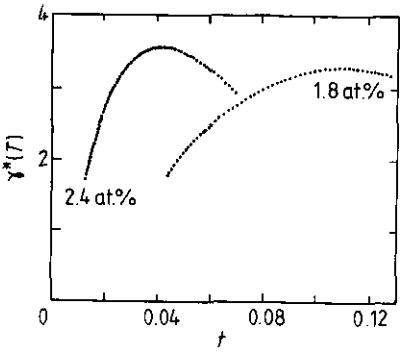

Figure 13. The Kouvel–Fisher susceptibility exponent $\gamma^*(T)$ plotted against reduced temperature t for the 1.8 and 2.4 at.% samples.

$\beta^*)^{-1} = 0.50$ for $t_m > 1.5 \times 10^{-2}$ ($\mu_0 H_i > 3$ mT), and with only a single point at lower t_m it would be very speculative to attribute the fall in t_m at low field to an increase in $(\gamma^* + \beta^*)^{-1}$ toward HM results. Data for the 2.4 at.% Fe sample, also shown in figures 11 to 13, display similar systematics, as do those from all specimens with 1.6 at.% Fe or more (see table 1).

4. Summary and conclusions

The data presented above are consistent with the 1.4 at.% sample being regarded as a nearly ideal system, the asymptotic exponent values being close to those predicted by the isotropic, three-dimensional HM. Within such a picture this sample would be described as one with interacting localized giant moments centred at the Fe sites; the interactions between such moments can be described by an exchange-coupling distribution in which the ratio of the first (J_0) to second moment (ΔJ) is large (i.e. a narrow distribution). Such a description agrees with the physical picture emerging from neutron-scattering experiments [19, 40], i.e. considerable homogeneity in the polarization of the exchange-enhanced d bands is established between 1 and 2 at.% Fe, presumably leading to a well defined J_0 with little fluctuation (ΔJ small)†. By contrast, in the 0.35 at.% sample there is clear evidence for substantial exchange-bond disorder; this is an expected result as the d band polarization is quite inhomogeneous, leading to considerable fluctuations

† Proponents of an itinerant-model description of this system might argue that the homogeneity of the d band polarization at this composition is the reason for the near-ideal behaviour of the 1.4 at.% specimen. A detailed comparison of neutron-scattering data from dilute PdFe and amorphous Fe_xZr_{1-x} ($x \simeq 0.9$) (which, while exhibiting localized HM exponents, appears as a more likely example of an itinerant d band system) might therefore prove interesting.

about the mean coupling strength. Despite these fluctuations, the data are consistent with asymptotic values for both γ and β being close to model predictions (in agreement with the Harris criterion, as $\alpha = 2 - 2\beta - \gamma = -0.12 < 0$); however, the low-field estimate for $\delta^*(H) = 3.4 \pm 0.1$ ($\mu_0 H_i < 1.5$ mT) is well below model values ($\delta = 4.80$). While estimates for the internal field become increasingly uncertain when this field falls below 0.1 mT, the ratio $J_0/\Delta J$ characterizing the exchange-bond distribution would need to be close to unity to produce significant increases in $\delta^*(H)$ below 0.1 mT. At first consideration this may not appear unreasonable, since the ratio $J_0/\Delta J$ has been estimated at $\simeq 1.1$ for (Pd+0.35 at.% Fe)+5 at.% Mn [41,42]; however, in this latter sample $\delta^*(H) = 4.1 \pm 0.1$ for $\mu_0 H_i \leqslant 10^2$ mT [22,42].

For samples containing 1.6 at.% Fe or more, neutron data indicate an increasingly homogeneous d band polarization. The corresponding exchange coupling would then be expected to exhibit progressively smaller fluctuations ΔJ. This latter expectation conflicts with the present data, which indicate, via figures 11 to 13, substantial exchange-bond disorder. We infer therefore that there should be some additional coupling mechanism which induces this disorder, and suggest that the most likely mechanism is near-neighbour direct exchange. While direct exchange is also expected to produce ferromagnetic coupling [43], if the characteristic strength of this coupling $J_0(\text{NN})$ is different from that for indirect coupling via the d band $J_0(\text{d})$, then a bimodal exchange distribution will develop with spectral-weight shifting from $J_0(\text{d})$ to $J_0(\text{NN})$ with increasing Fe concentration. Whether such a distribution would eventually evolve at higher Fe composition into one centred around $J_0(\text{NN})$ with little width (giving a well defined critical behaviour, as in the 1.4 at.% alloy) is uncertain, as are the exponents characterizing the associated transition. Existing data at much higher Fe concentration (Pd_3Fe) are contradictory [4,6], with more recent measurements favouring mean-field exponent values (still accompanied by clear manifestations of exchange-bond disorder [6]). The data reproduced in figure 11 for the 2.4 at.% sample might be taken as supporting the more recent results, as $\delta^*(H) = 3.0 \pm 0.1$ for $1 \leqslant \mu_0 H_i \leqslant 3.5$ mT; however, this ignores the presence of anisotropy which prevents observations at lower field (thus possibly masking further increase in $\delta^*(H)$).

Nevertheless the introduction of near-neighbour direct exchange could qualitatively explain the occurrence of exchange disorder in samples with 1.6 at.% Fe or more, and it is also consistent with the behaviour in figure 1. The change in the linear increase of T_C with c near 2 at.% noted in the introduction would correspond to a change in the dominant contribution to the exchange distribution from $J_0(\text{d})$ to $J_0(\text{NN})$; indeed figure 1 suggests that the strength of the latter is less than that of the former. That this change initially appears above 1.4 at.% Fe (at least as far as the detailed behaviour of the critical peaks is concerned; these appear to be somewhat more sensitive than bulk properties such as the moment/impurity and T_C) would require direct exchange to be effective out to possibly third-nearest neighbour (42 sites in an FCC lattice). While this might appear, at first sight, to be rather long-ranged, it is in agreement with the spatial extent deduced for Mn–Mn direct/near-neighbour exchange in PdMn [44].

Acknowledgments

We are pleased to acknowledge grants from the Natural Sciences and Engineering Research Council of Canada and the Research Board of the University of Manitoba in support of this work.

References

[1] Nieuwenhuys G J 1975 *Adv. Phys.* **24** 515
[2] Peters R P, Buchal Ch, Kubota M, Mueller R M and Pobell F 1984 *Phys. Rev. Lett.* **53** 1108
[3] Webb R A, Crabtree G W and Vuillemin J J 1979 *Phys. Rev. Lett.* **43** 796
[4] Kouvel J S and Comly J B 1971 *Critical Phenomena in Alloys, Magnets and Superconductors* ed R E Mills *et al* p 437
[5] Craig P P, Perisho R C, Segnan R and Steyert W A 1965 *Phys. Rev.* **135A** 1460
[6] Seeger M and Kronmüller H 1989 *J. Magn. Magn. Mater.* **78** 393
[7] Schroeder P A and Uher C 1978 *Phys. Rev.* B **18** 3884
[8] Andrianov V A, Kozin M G, Pentin A Yu, Shpinel V S, Gor'kov V P and Mechenov A S 1987 *Sov. Phys.–Solid State* **29** 1348
[9] Kornik K, Kunkel H P and Roshko R M 1988 *J. Appl. Phys.* **64** 5619
[10] Verbeek B H, Nieuwenhuys G J, Mydosh J A, van Dijk C and Rainford B D 1980 *Phys. Rev.* B **22** 5426
[11] Mydosh J A, Budnick J I, Kawatra M P and Skalski S 1968 *Phys. Rev. Lett.* **21** 1346
[12] Grassie A D C, Swallow G A, Williams G and Loram J W 1971 *Phys. Rev.* B **3** 4154
[13] Skalski S, Kawatra M P, Mydosh J A and Budnick J I 1970 *Phys. Rev.* B **2** 3613
[14] Smith T F, Gardner W G and Montgomery H 1970 *J. Phys. C: Solid State Phys.* **3** S370
[15] Williams G and Loram J W 1979 *J. Phys. Chem. Solids* **30** 1827
[16] Long P D and Turner R E 1970 *J. Phys. C: Solid State Phys.* **2** S127
[17] Minnari I 1959 *Prog. Theor. Phys.* **22** 335
[18] Colp M E and Williams G 1972 *Phys. Rev.* B **5** 2599
[19] Low G G and Holden T M 1966 *Proc. Phys. Soc.* **89** 119
[20] Maartense I 1970 *Rev. Sci. Instrum.* **41** 657
[21] Ma H, Kunkel H P and Williams G 1991 *J. Phys.: Condens. Matter* **3** 5563
[22] Williams G 1992 *Magnetic Susceptibility of Superconductors and Other Spin Systems* ed R A Hein *et al* (New York: Plenum)
[23] Bozorth R M 1951 *Ferromagnetism* (New York: van Nostrand)
Heck C 1974 *Magnetic Materials and their Applications* (London: Butterworth)
[24] Kunkel H P, Roshko R M, Ruan W and Williams G 1991 *Phil. Mag.* B **63** 1213
[25] Stanley H E 1971 *Introduction to Phase Transitions and Critical Phenomena* (Oxford: Clarendon)
[26] LeGuillou L C and Zinn-Justin J 1980 *Phys. Rev.* B **21** 3976
[27] Kunkel H P, Roshko R M and Williams G 1988 *Phys. Rev.* B **37** 5880
[28] Roshko R M and Williams G 1984 *J. Phys. F: Met. Phys.* **14** 703
[29] Kornik K, Kunkel H P, Roshko R M and Williams G 1990 *Solid State Commun.* **76** 993
[30] Widom B 1965 *J. Chem. Phys.* **43** 3898
[31] Kouvel J S and Fisher M E 1964 *Phys. Rev.* A **136** 1626
[32] Gaunt P, Ho S C, Williams G and Cochrane R W 1981 *Phys. Rev.* B **23** 251
[33] Kaul S N 1985 *J. Magn. Magn. Mater.* **53** 5
[34] Wang Z, Kunkel H P and Williams G 1990 *J. Phys.: Condens. Matter* **2** 4173
[35] Senoussi S, Campbell I A and Fert A 1977 *Solid State Commun.* **2** 269
[36] Campbell I A, Fert A and Jaoul O 1970 *J. Phys. C: Solid State Phys.* **3** S95
[37] Friederich A and Fert A 1974 *Phys. Rev. Lett.* **33** 1214
[38] Ho S C, Maartense I and Williams G 1981 *J. Phys. F: Met. Phys.* **11** 699
[39] Ho S C, Maartense I and Williams G 1981 *J. Phys. F: Met. Phys.* **11** 1107
[40] Stringfellow M W 1968 *J. Phys. C: Solid State Phys.* **1** 1699
[41] Verbeek B H, Nieuwenhuys G J, Stocker H and Mydosh J A 1978 *Phys. Rev. Lett.* **40** 586
[42] Kunkel H P and Williams G 1988 *J. Magn. Magn. Mater.* **75** 98
[43] Moriya T 1967 *Proc. Int. School of Physics, Enrico Fermi, Course XXXVII* (New York: Academic)
[44] Smit J J, Nieuwenhuys G J and de Jongh L J 1979 *Solid State Commun.* **30** 243